

Supporting Information

Modular O₂ Electroreduction Activity in Triphenylene-Based Metal-Organic Frameworks

Elise M. Miner,[†] Lu Wang,[‡] Mircea Dincă^{*†}

[†]Department of Chemistry, Massachusetts Institute of Technology, Cambridge, Massachusetts 02139, United States

[‡]Key Laboratory of Cluster Science, Ministry of Education of China, Beijing Key Laboratory of Photoelectronic/Electrophotonic Conversion Materials, School of Chemistry, Beijing Institute of Technology, Beijing 100081, P. R. China

mdinca@mit.edu

Table of Contents:

Materials	S3
Methods.....	S3
Figure S1. CVs of the triphenylene MOFs under N ₂	S9
Figure S2. CVs of Cu ₃ (HITP) ₂ showing deactivation under O ₂	S10
Figure S3. CVs of the trigonal MOFs on ITO	S11
Table S1. % current retained during ORR with MOFs after 8 h	S12
Figure S4. RRDE studies during ORR with the triphenylene MOFs	S13
Figure S5. Faradaic efficiencies of ORR with the triphenylene MOFs	S14
Figure S6. Koutecky-Levich plots from ORR with the triphenylene MOFs	S15
Table S2. Exchange current density values for ORR with MOFs	S16
Figure S7. ORR order in [O ₂] with the triphenylene MOFs	S17
Table S3. Slopes for the ORR order in [O ₂] plots.....	S18
Figure S8. pH-dependent redox activity of Cu ₃ (HHTP) ₂ under N ₂	S19

Figure S9. pH-dependent redox activity of $\text{Cu}_3(\text{HITP})_2$ under N_2	S20
Figure S10. Redox inactivity of the trigonal MOFs under N_2	S21
Supplementary Notes and References	S22

Experimental

Materials

KOH (99.99% trace metals), NaCl (99.99% trace metals), and HClO₄ (99.99% trace metals) were purchased from Sigma-Aldrich. The aqueous electrolytes were made from Milli-Q water (18 MΩ). Oxygen gas was purchased from Airgas (99.8% purity). Reference electrodes were purchased from CH Instruments. Indium tin oxide (ITO) working electrodes were purchased from Delta Technologies, Ltd. Pt gauze (100 mesh, 99.9% metal basis) and wires ($\phi = 0.404$ mm, annealed, 99.9% metal basis, and $\phi = 0.5$ mm dia., hard, 99.95% metal basis) comprising the auxiliary electrode were purchased from Alfa Aesar. Rotating disk electrode and Pt rotating ring disk electrode assemblies (1 mm width Pt) with glassy carbon working electrode inserts (5 mm diameter) were purchased from Pine Research Instrumentation. 2,3,6,7,10,11-hexahydroxytriphenylene (HHTP, 95%) was purchased from Acros Organics and recrystallized from ethanol before use. 5 wt% Nafion 117 solution in isopropanol was purchased from Sigma Aldrich. 2mm and 8mm slits were used during the powder X-ray diffraction data collection, with a scan rate of 0.02 degrees·second⁻¹ and a dwell time of 0.2 seconds·step⁻¹.

Methods

Electrochemical measurements. The Pt auxiliary electrode was cleaned by submersion in concentrated HCl followed by sonication for 5min, washing with Milli-Q water, and drying under a stream of air before each experiment. Glassy carbon working electrodes were cleaned by submersion in concentrated HCl followed by sonication for 5min, washing with Milli-Q water, and drying under a stream of air. The glassy carbon working electrodes were then sequentially polished with 1, 0.3 and 0.05 μm diameter alumina powder from BASI. Unless otherwise noted,

all electrochemical experiments were executed with a Bio-Logic SP200 potentiostat / galvanostat in a custom 2-compartment electrochemical cell. Rotating disk electrode studies were conducted with a Bio-Logic VMP3 potentiostat / galvanostat and a Pine Research Instrumentation Modulated Speed Rotator. Unless otherwise specified, internal resistance of the electrolyte was measured with the Bio-Logic SP200 potentiostat / galvanostat by passing $-100 \mu\text{A}$ current, and iR drop correction was applied. Generally, the resistance of the electrolyte was measured to be $\sim 20 \Omega$. Prior to data collection under a given atmosphere (N_2 or O_2), the electrolyte was sparged for 20 minutes with that gas and sparged continuously during data collection. For the pH 13 (0.1 M KOH) electrolyte, a Hg/HgO reference electrode (1.0 M KOH) was used and for the pH 8 electrolyte (0.1 M NaCl), a Ag/AgCl electrode was used (1.0 M NaCl). Unless otherwise noted, cyclic voltammetry data was collected while rotating the working electrode at 2,000 r.p.m. and cycling at $5 \text{ mV}\cdot\text{s}^{-1}$.

Synthesis of the HITP MOFs. The 2,3,6,7,10,11-hexaaminotriphenylene (HATP) ligand and $\text{Ni}_3(\text{HITP})_2$ was synthesized as described previously.¹ $\text{Cu}_3(\text{HITP})_2$ was synthesized as described previously.²

Synthesis of the HHTP MOFs. Co, Ni, and $\text{Cu}_3(\text{HHTP})_2$ were synthesized as reported previously.³

Deposition of the MOFs onto the electrodes. Catalyst inks were prepared by dispersing 2 mg of the catalyst in a volume of 1:1 Millipore water:isopropyl alcohol (190 μL) with 10 μL of 5 wt% Nafion. The ink solution was then sonicated for 25 minutes to get a uniform suspension. 2 x 5 μL of the catalyst ink was deposited on the polished or otherwise cleaned electrodes and dried under vacuum before use.

Determination of the MOF-mediated ORR order in [O₂]. The electrolyte was sparged with O₂ for 20 minutes then CV under O₂ was taken from 0 V versus OCP to -0.4 V vs Ag/AgCl. The [O₂] order data was collected by holding the potential at from the ORR onset potential to approximately -0.4 V vs Ag/AgCl for two minutes at each potential (refer to Figure S6 for the exact potentials for each analogue), going from 10% O₂ / 90% N₂ to 100% O₂ / 0% N₂ electrolyte atmosphere at each potential value, with sparging the new atmosphere for 20 minutes before data collection. For each potential, a log(I) versus log(partial pressure O₂) plot was made to extrapolate the order in O₂ and observe the dependence of the order on the potential.

Koutecky-Levich and Tafel studies. Collection of the Koutecky-Levich and Tafel data was previously described.⁴ CV in pH 8 electrolyte (0.1 M NaCl) (5 mV·s⁻¹) under N₂ atmosphere then under O₂ atmosphere was conducted from 0 V versus OCP to -0.4 V versus Ag/AgCl (ORR potential range) with the unmodified glassy carbon electrode then the MOF-modified glassy carbon electrode. Potentiostatic measurements were conducted from the ORR onset potential to the potential at which diffusion limitations prevented steady current (refer to Figure S5 for exact potentials for each analogue) in increments of 20 mV under O₂ atmosphere. Each potential was held for 2 minutes. This was conducted three times, with altering rotation speeds to extrapolate the diffusion coefficient. The electrode was rotated at 625, 816, and 1,189 r.p.m., respectively. This allowed for elimination of mass transport limitations when analyzing Tafel behavior *via* generation of the activation-controlled Tafel plot.

ORR [H⁺] order study. Potential versus Ag/AgCl was measured at a constant current $I = -10 \mu\text{A}$ while varying the pH from 13.5 to 8.0 in the 0.10 M KOH electrolyte titrated with 1.0 M HClO₄

in the presence of O₂ while rotating at 2,000 r.p.m. Each potential required to pass -10 μA at a given pH was allowed to reach steady state before more titrant was added. Potential versus pH was plotted and the slope was divided by the Tafel slope to obtain the ORR order in [H⁺].

Probing the pH-dependent redox potentials of the MOFs. Cyclic voltammetry (CV) was run with an unmodified glassy carbon electrode from E = -1.1 V to E = 0.7 V versus SCE, then the first MOF-modified electrode was used in pH 13.6, and CV was run scanning cathodically first from E = -1.1 V to E = 0.7 V versus SCE for two cycles (electrode 1). The electrolyte was then titrated to a lower pH (refer to Figures S7 and S8 for the exact pH environments studied for each analogue) an unused MOF-modified working electrode (electrode 2) was installed, and the procedure was repeated. The electrolyte was then titrated to yet a lower pH, and the same procedure for electrode 1 was used on the new electrode 3. This procedure was repeated with a minimum of 5 electrodes (at least 5 pH values) for each redox-active analogue. The potentials associated with the peak currents passed in the MOF oxidation events were plotted versus pH. Since Co₃(HHTP)₂ and Ni₃(HHTP)₂ showed no redox activity, CV was only collected in pH 8.

Stability testing MOFs in pH 13 electrolyte. CV was conducted under O₂ with the MOF-modified glassy carbon electrode for 50 cycles from 0.1 V to -0.3 V versus Hg/HgO to monitor loss in ORR activity with progressing cycles. For potentiostatic durability tests, 1 CV cycle was collected for each sample to determine the activation-controlled ORR potential window. The potential was then held within that potential window for 8 hours and the percent current retained during ORR in the activation-controlled region was calculated.

Faradaic efficiency for 2e⁻ ORR with MOFs. The potential on the MOF-modified disk was held from 0.67 V to 0.38 V vs RHE in pH 8, with more cathodic potentials applied every two minutes in increments of 20 mV under an O₂ atmosphere while rotating at 2,000 r.p.m. Simultaneously, the Pt ring potential was held at 0.53 V vs SCE (1.23 V vs RHE), sufficient to re-oxidize H₂O₂ on the Pt surface but not H₂O. Once the cathodic current from the disk and the anodic current from the ring was collected, the faradaic efficiency (FE) for 2e⁻ ORR was calculated using the following equation:

$$FE_{H_2O_2} = \frac{I_{ring}}{0.18 \cdot I_{disk}} \cdot 100$$

where I_{ring} = the average Pt ring current taken from the last 10 seconds at a given potential, I_{disk} = the average MOF-modified disk current taken from the last 10 seconds at a given potential, and 0.18 = the collection efficiency of the Pt ring, which had been calibrated with potassium ferro / ferricyanide.

Electroactive surface area (ESA) measurements. In 0.1 M NaCl, cyclic voltammograms of the MOF were collected under N₂ in the non-faradaic potential range of 0 V to 0.05 V vs SCE at scan rates (v) of 10, 8, 6, 4, and 2 mV/s, respectively. Capacitive current (I) at 0.025 V vs SCE was plotted versus v , giving a slope that represented the double layer capacitance in Farads. This was divided by the geometric surface area of the electrode to approximate the electroactive surface area (F·m⁻²).

Pressed pellet conductivity. Conductivity measurements were executed using a home-built press previously described.⁵ MOF powder was pressed between two stainless steel rods (2 mm diameter) inside of a glass capillary. Pellet resistance was measured with a multimeter.

Additional Figures

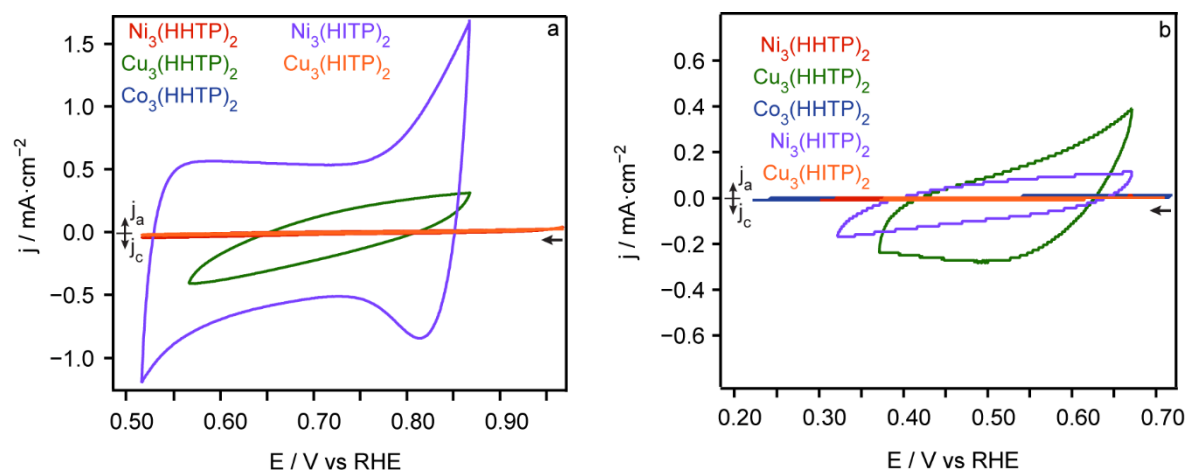


Figure S1. Cyclic voltammograms of the triphenylene MOFs under N_2 in a) pH 13 and b) pH 8.

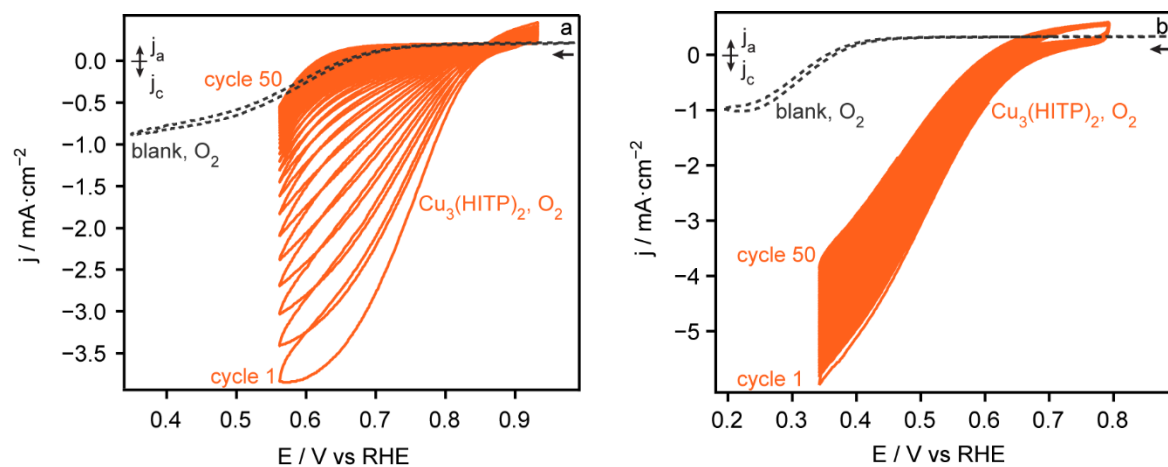


Figure S2. Cyclic voltammograms of $\text{Cu}_3(\text{HITP})_2$ under O_2 in a) pH 13 and b) pH 8, showing the loss of activity due to instability of the catalyst. “Blank” indicates the background current from the unmodified glassy carbon electrode.

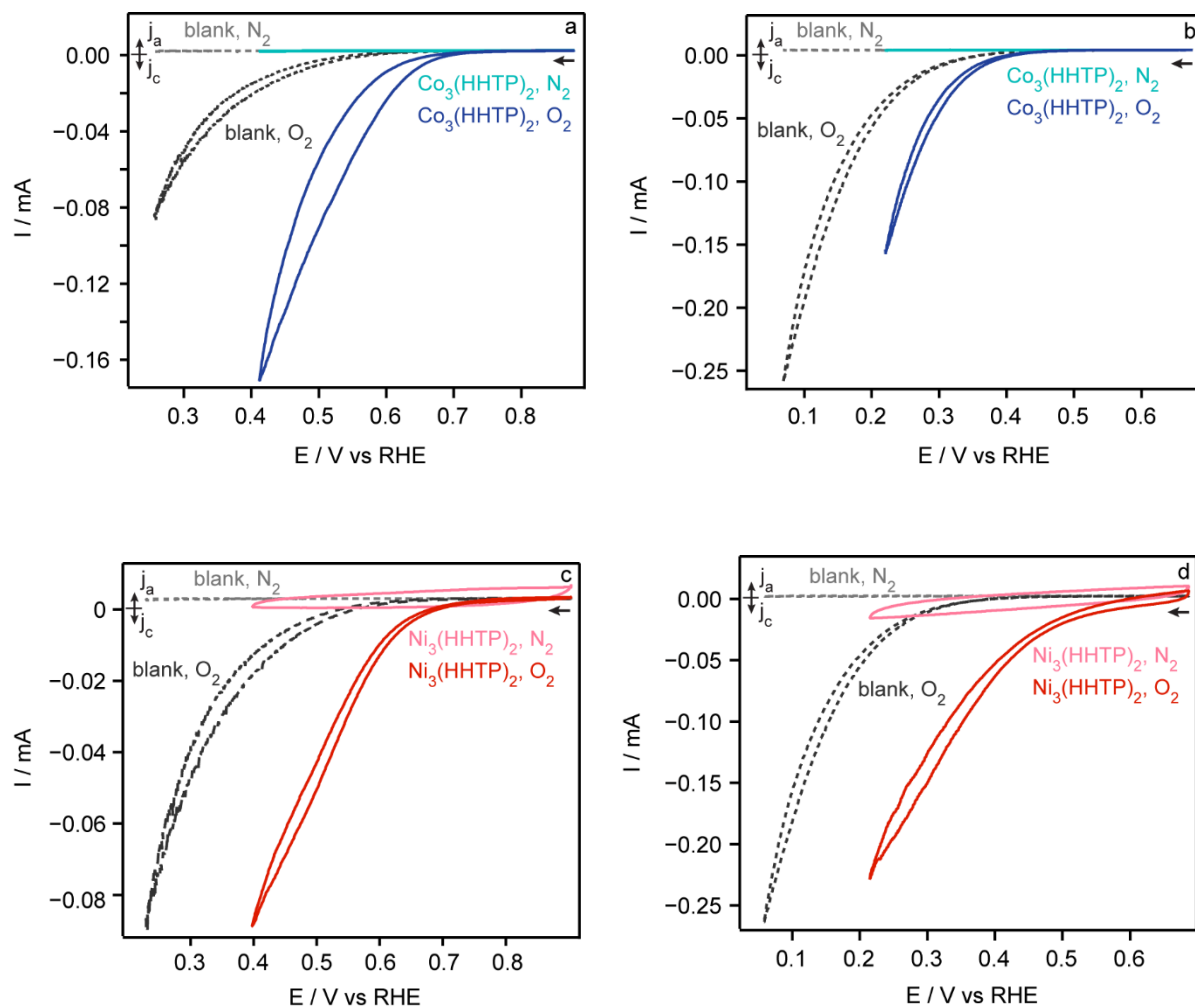


Figure S3. Cyclic voltammograms of $\text{Co}_3(\text{HHTP})_2$ deposited on indium tin oxide (blank) in a) pH 13 and b) pH 8, and of $\text{Ni}_3(\text{HHTP})_2$ in c) pH 13 and d) pH 8 under N_2 (lighter colors) and O_2 (darker colors).

Table S1. % current retained during potentiostatic ORR in pH 13 after 8 hours.

MOF	% current retained after 8 hours ORR
Ni ₃ (HITP) ₂	88 ⁴
Cu ₃ (HITP) ₂	6
Co ₃ (HHTP) ₂	62
Ni ₃ (HHTP) ₂	58
Cu ₃ (HHTP) ₂	73

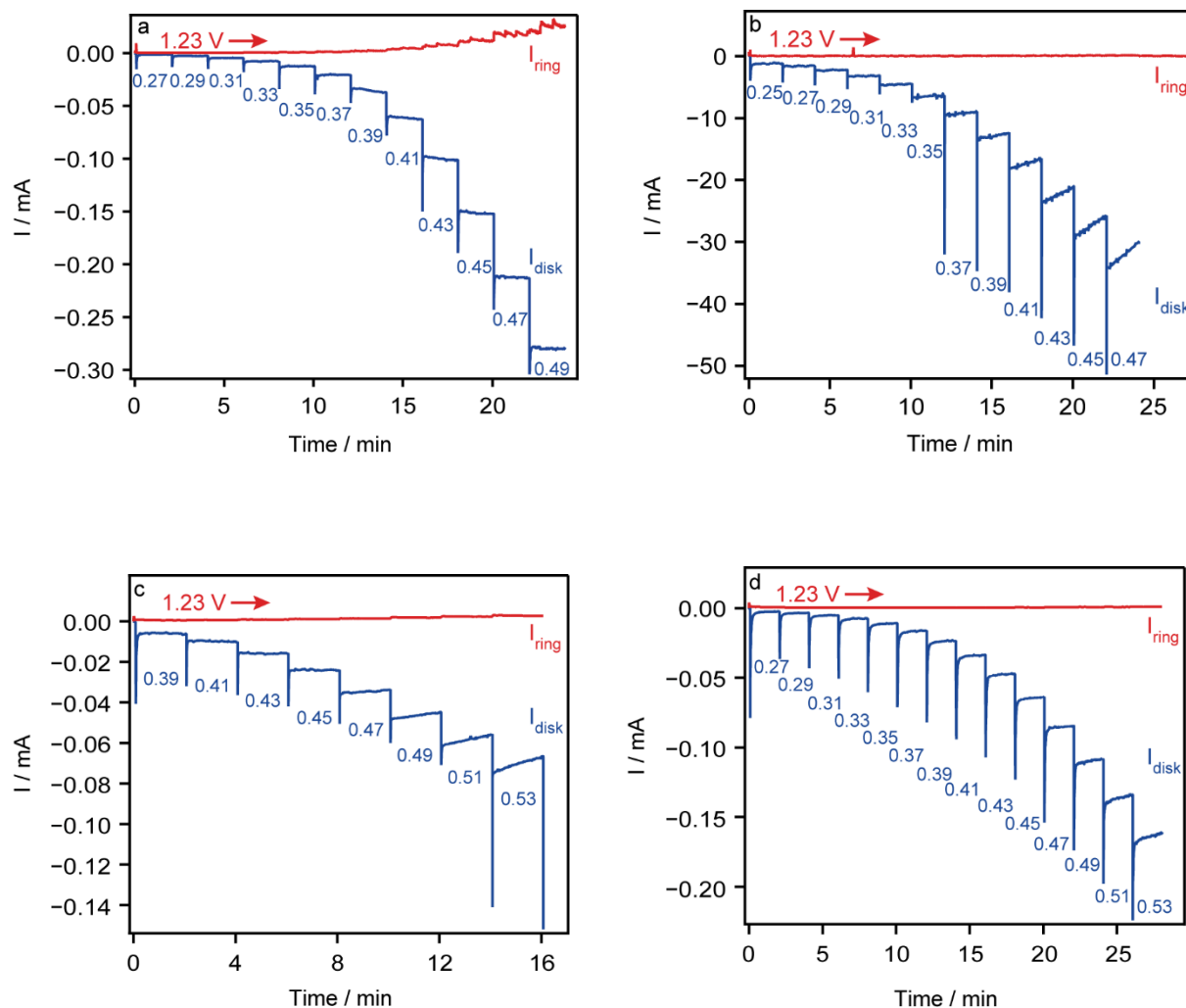


Figure S4. RRDE data for ORR with a) $Ni_3(HITP)_2$, b) $Co_3(HHTP)_2$, c) $Ni_3(HHTP)_2$, and d) $Cu_3(HHTP)_2$ in pH 8. Red indicates the ring current and blue indicates the disk current. Ring held at a constant potential of 1.23 V vs RHE. Disk potentials are listed as ORR overpotentials (η , V).

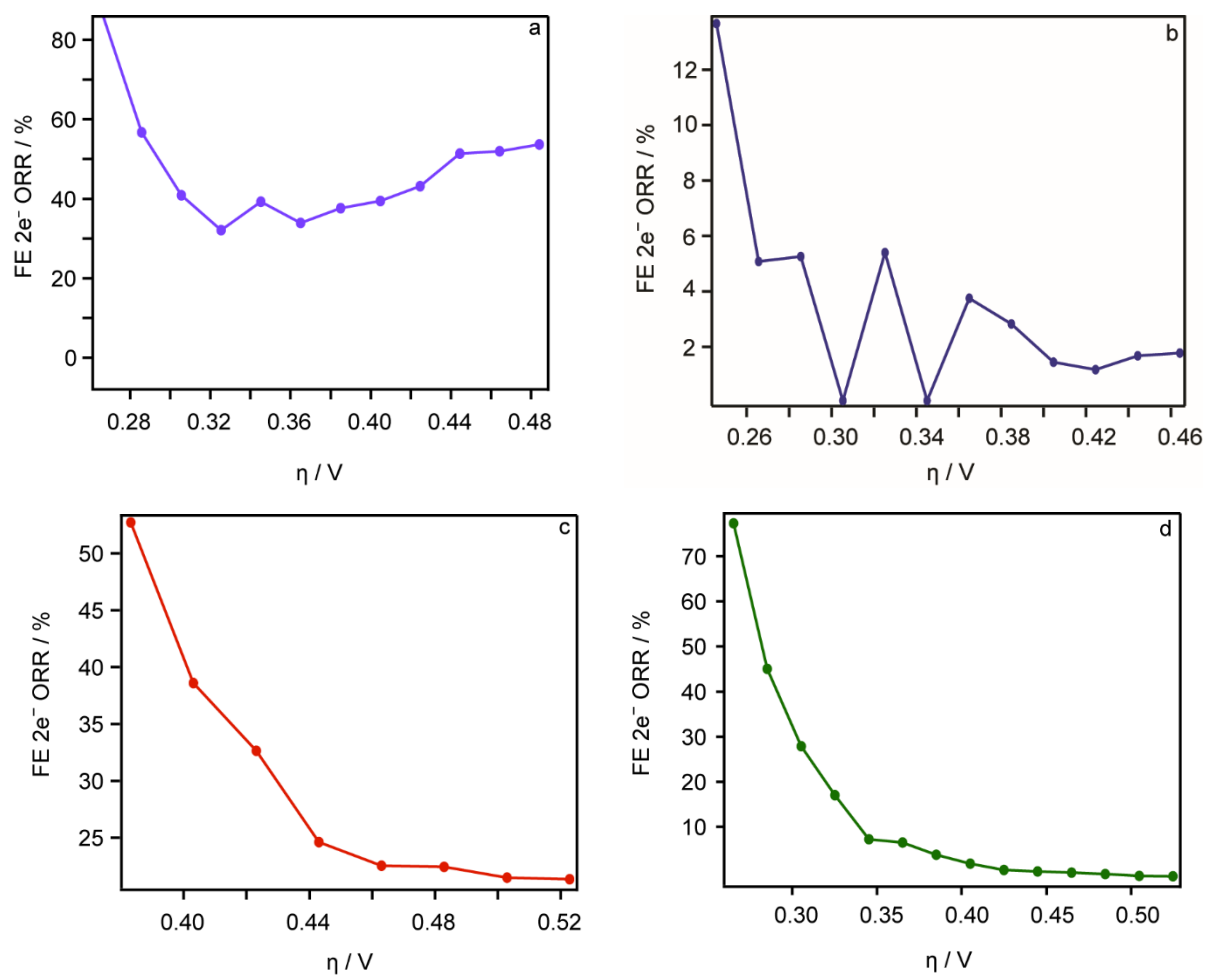


Figure S5. Faradaic efficiency (FE) for 2e⁻ ORR as a function of ORR overpotential with a) $\text{Ni}_3(\text{HITP})_2$, b) $\text{Co}_3(\text{HHTP})_2$, c) $\text{Ni}_3(\text{HHTP})_2$, and d) $\text{Cu}_3(\text{HHTP})_2$ in pH 8.

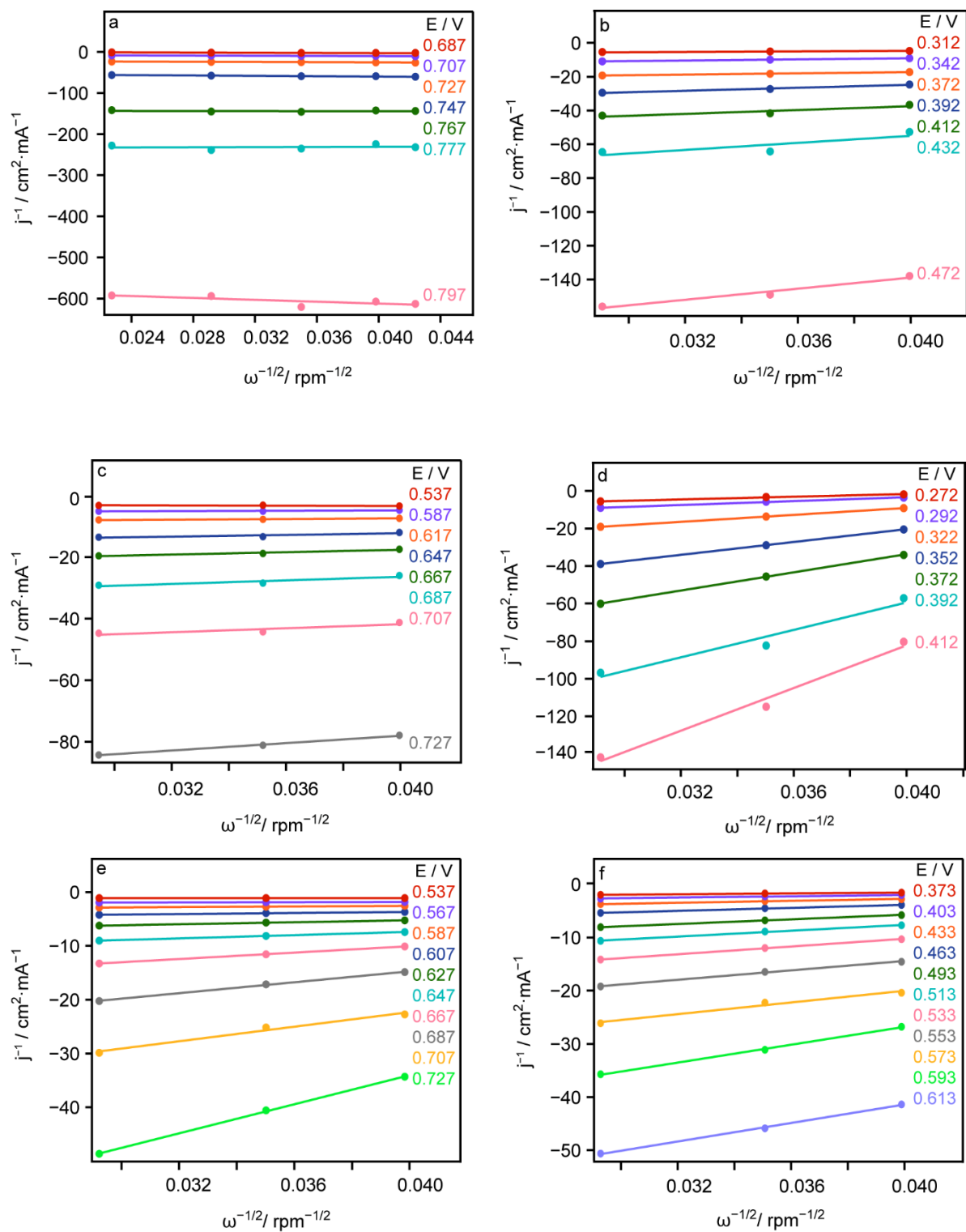


Figure S6. Koutecky-Levich plots (E vs RHE) used to generate the activation-controlled Tafel plots in Figure 3. $\text{Co}_3(\text{HHTP})_2$ in pH 13 and 8 is shown in a and b respectively, $\text{Ni}_3(\text{HHTP})_2$ in pH 13 and 8 is shown in c and d respectively, and $\text{Cu}_3(\text{HHTP})_2$ in pH 13 and 8 is shown in e and f, respectively. Refer to Reference 13 in the main text for the Koutecky-Levich plots for $\text{Ni}_3(\text{HHTP})_2$.

Table S2. Exchange current density values (j_0) as metrics for comparing ORR electrokinetics of the various MOF catalysts. Higher exchange current density is indicative of faster electrokinetics.

pH	MOF	Tafel equation	log(abs(j_0))	$j_0 / \text{mA}\cdot\text{cm}^{-2}$
13	Ni ₃ (HITP) ₂	$y = 0.128x + 0.458$	-3.5781	$2.64\cdot 10^{-4}$
13	Co ₃ (HHTP) ₂	$y = 0.081x + 0.664$	-8.1975	$6.35\cdot 10^{-9}$
13	Ni ₃ (HHTP) ₂	$y = 0.107x + 0.714$	-6.6729	$2.12\cdot 10^{-7}$
13	Cu ₃ (HHTP) ₂	$y = 0.112x + 0.732$	-6.5357	$2.91\cdot 10^{-7}$
8	Ni ₃ (HITP) ₂	$y = 0.124x + 0.420$	-3.3871	$4.10\cdot 10^{-4}$
8	Co ₃ (HHTP) ₂	$y = 0.122x + 0.741$	-6.0738	$8.44\cdot 10^{-7}$
8	Ni ₃ (HHTP) ₂	$y = 0.117x + 0.810$	-6.9231	$1.19\cdot 10^{-7}$
8	Cu ₃ (HHTP) ₂	$y = 0.176x + 0.648$	-3.6818	$2.08\cdot 10^{-4}$

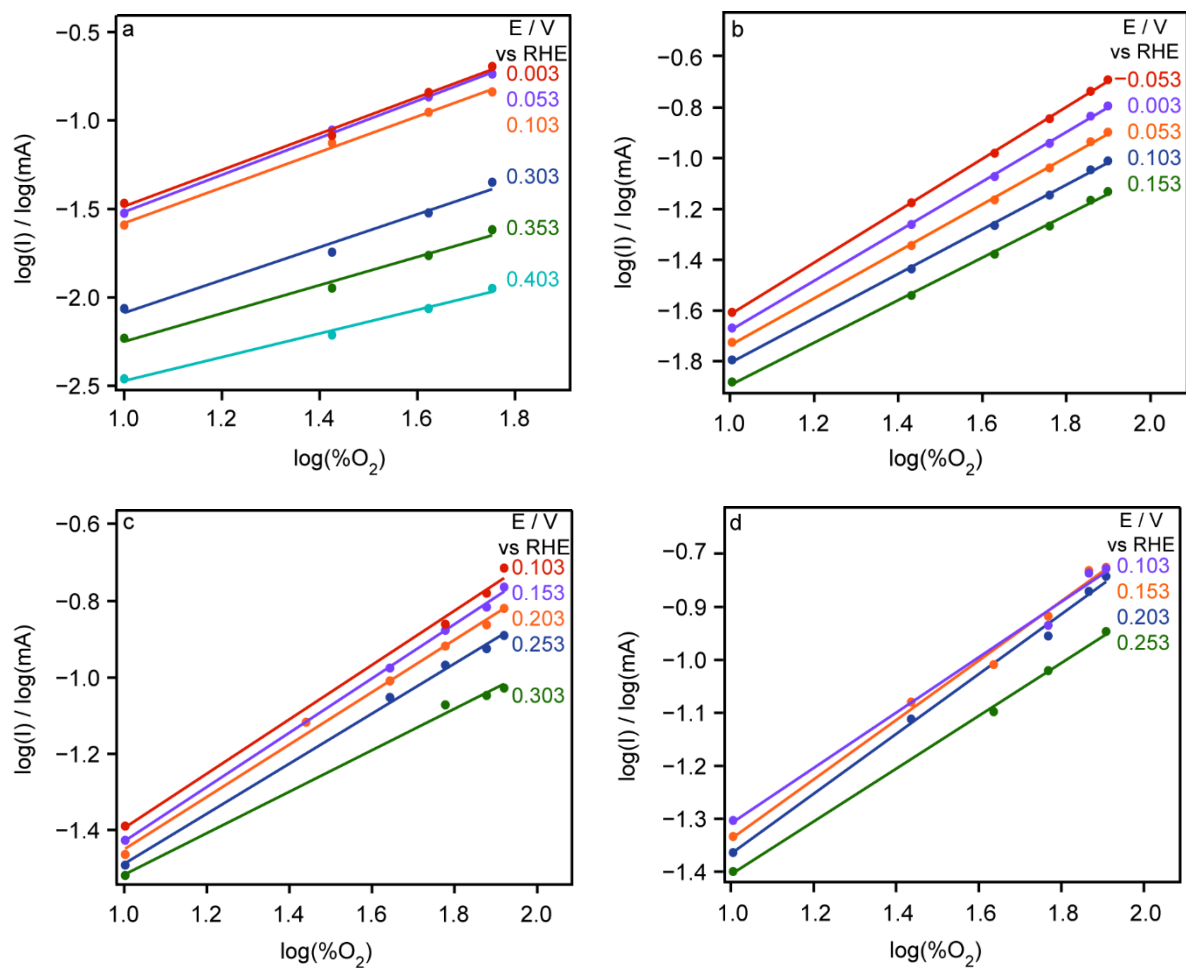


Figure S7. Potentiostatic [O₂] order data for a) $\text{Co}_3(\text{HHTP})_2$, b) $\text{Ni}_3(\text{HHTP})_2$, c) $\text{Cu}_3(\text{HHTP})_2$, and d) $\text{Cu}_3(\text{HITP})_2$ in pH 8. Refer to Reference 15 in the main text for the ORR [O₂] order data for $\text{Ni}_3(\text{HITP})_2$.

Table S3a. Corresponding slopes of the variable potential [O₂] order plots collected in pH 8 for Co₃(HHTP)₂ (Figure S7a).

E / V vs RHE	Slope
0.403	0.60
0.353	0.72
0.303	0.84
0.103	0.91
0.053	0.94
0.003	0.93

Table S3b. Corresponding slopes of the variable potential [O₂] order plots collected in pH 8 for Ni₃(HHTP)₂ (Figure S7b).

E / V vs RHE	Slope
0.153	0.80
0.103	0.84
0.053	0.88
0.003	0.93
-0.053	0.97

Table S3c. Corresponding slopes of the variable potential [O₂] order plots collected in pH 8 for Cu₃(HHTP)₂ (Figure S7c).

E / V vs RHE	Slope
0.303	0.52
0.253	0.62
0.203	0.65
0.153	0.68
0.103	0.68

Table S3d. Corresponding slopes of the variable potential [O₂] order plots collected in pH 8 for Cu₃(HITP)₂ (Figure S7d).[‡] See Supplementary Note regarding this [O₂] order data for this analogue.

E / V vs RHE	Slope
0.253	0.47
0.203	0.53
0.153	0.53
0.103	0.49

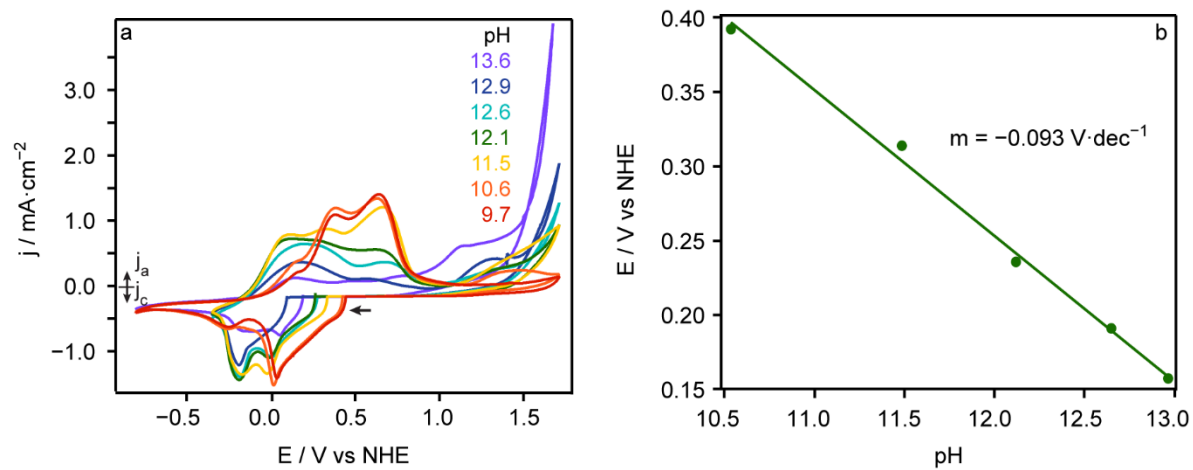


Figure S8. a) pH-dependent redox activity of $\text{Cu}_3(\text{HHTP})_2$ under N_2 atmosphere, and b) plot of the peak oxidation potential 1 of $\text{Cu}_3(\text{HHTP})_2$ as a function of pH.

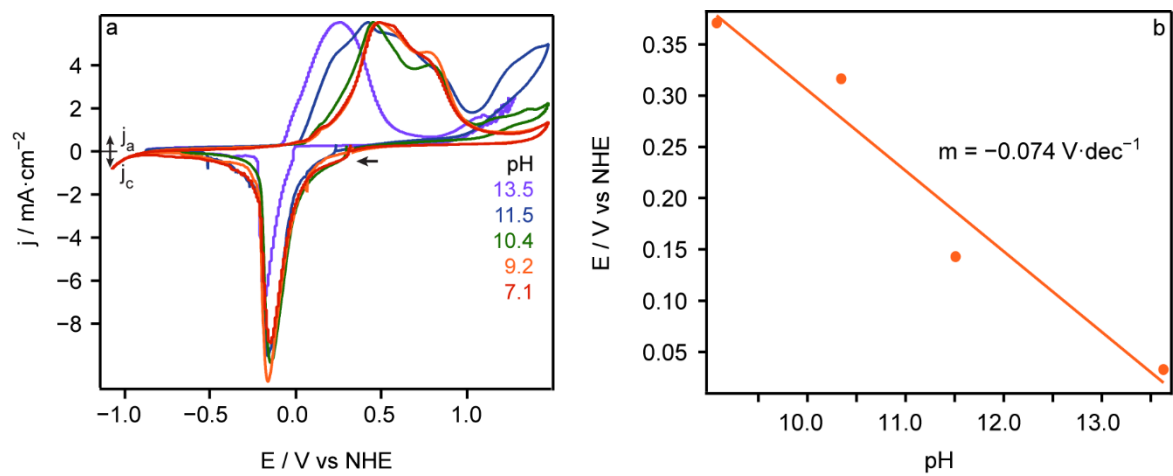


Figure S9. a) pH-dependent redox activity of $\text{Cu}_3(\text{HITP})_2$ under N_2 atmosphere, and b) plot of the peak oxidation potential 1 of $\text{Cu}_3(\text{HITP})_2$ as a function of pH.

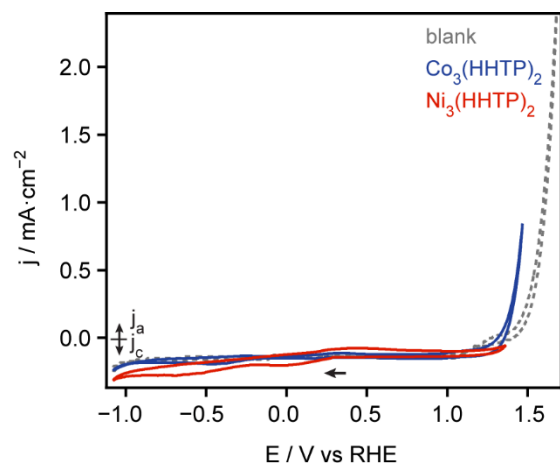


Figure S10. Cyclic voltammograms of the trigonal, redox-inactive MOFs $\text{Co}_3(\text{HHTP})_2$ and $\text{Ni}_3(\text{HHTP})_2$ under N_2 , on a glassy carbon electrode (blank) in 0.1 M NaCl.

Supplementary Notes and References

‡ Although the $\delta\log(I)/\delta\log(\%O_2)$ slope reflecting the ORR order in $[O_2]$ with $Cu_3(HITP)_2$ is reported here as 0.47-0.53, this may be quantitatively inaccurate due to the instability of this analogue to O_2 . This data was included to reflect that ORR with $Cu_3(HITP)_2$, as with all other analogues reported here, exhibits a non-zero order in $[O_2]$.

- 1 D. Sheberla, L. Sun, M. A. Blood-Forsythe, S. Er, C. R. Wade, C. K. Brozek, A. Aspuru-Guzik and M. Dincă, *J. Am. Chem. Soc.*, 2014, **136**, 8859–8862.
- 2 M. G. Campbell, D. Sheberla, S. F. Liu, T. M. Swager and M. Dincă, *Angew. Chemie Int. Ed.*, 2015, **54**, 4349–4352.
- 3 M. Hmadeh, Z. Lu, Z. Liu, F. Gándara, H. Furukawa, S. Wan, V. Augustyn, R. Chang, L. Liao, F. Zhou, E. Perre, V. Ozolins, K. Suenaga, X. Duan, B. Dunn, Y. Yamamoto, O. Terasaki and O. M. Yaghi, *Chem. Mater.*, 2012, **24**, 3511–3513.
- 4 E. M. Miner, T. Fukushima, D. Sheberla, L. Sun, Y. Surendranath and M. Dincă, *Nature Commun.*, 2016, **7**, 10942-10949.
- 5 F. Wudl and M. R. Bryce, *J. Chem. Educ.*, 1990, **67**, 717.